

Computer Modeling of Loran Additional Secondary Factors

Janet M. Blazyk, *Ohio University*

David W. Diggle, *Ohio University*

Abstract

Propagation phase delays known as additional secondary factors (ASFs) can occur when a Loran signal traverses non-seawater terrain. Accurate navigation using Loran requires precise timing; hence there is a need to determine ASF values that may be stored in a Loran receiver and subsequently used to refine the position solution. The BALOR computer program models Loran signal propagation, including the effects of ground conductivity and topography, thus providing predictions of received ASF values. This paper presents a review of the equations and algorithms currently used by the BALOR model, with illustrations and examples. Results from recent preliminary validation studies comparing measured and predicted ASF values are also shown.

1 Introduction

The Long Range Navigation system, or Loran, has historically been used for navigation over seawater. This was quite successful, as the speed of signal propagation over seawater was sufficiently well-characterized to meet the navigation needs of ocean-going vessels. Although today the Global Positioning System (GPS) has become a preferred navigation method for land, sea, and air, due to its ease of use, reliability, and accuracy, there is renewed interest in determining whether Loran could be enhanced in order to serve as a backup to GPS. Since Loran is a high-power, low-frequency, land-based system, it is an ideal complement to the low-power, high-frequency, space-based GPS system, making it unlikely to share a common failure mode.

The Loran signal is capable of propagating over large distances via groundwave and skywave, although the skywave is generally not used for navigation. Accurate position determination depends on precise timing of the received signals from several known transmitters and calculation of distance from each transmitter based on the time and speed of propagation. This operation is complicated by the fact that the signal does not travel at a uniform velocity, but is influenced by the terrain and atmosphere over its propagation path.

The overall signal delay is the sum of three components: primary factor (PF), secondary factor (SF), and additional secondary factor (ASF). The PF accounts for the speed of propagation through the atmosphere, and is easily calculated. The SF accounts for the extra delay for a signal traveling over a spherical seawater surface, rather than over a perfectly-conducting plane. Although it seems to be accepted that the SF is a known function of distance, we will later point out some possible areas of concern. The ASF accounts for any additional delay caused by a signal path that is at least partly over terrain, rather than all seawater, as well as any other factors that may come into play.

ASFs are of particular concern because they are variable and difficult to predict, yet ignoring them could lead to lateral position errors of up to a nautical mile or more. It has been demonstrated that employing measured or predicted ASF values can greatly improve the navigation performance of a Loran receiver [1], [2]. In order to meet Required Navigation Performance (RNP) 0.3 accuracy requirements for non-precision approach and landing guidance, it is essential to have accurate ASF values. The best solution in this case may be direct measurement of ASFs at each airport. For enroute operations, the accuracy requirements will be less stringent, but the area to be covered will be much larger. Due to the impracticality of measuring ASFs throughout the Loran coverage area, it will be necessary to use a model to predict a grid of ASF values, which can then be corrected as needed by using specific measured values.

The BALOR computer program was developed by Paul Williams and David Last of the University of Wales, Bangor, UK [3], [4]. This software models Loran signal propagation, including the effects of ground conductivity and topography, thus providing predictions of received ASF values over a specified path or area. The Avionics Engineering Center at Ohio University undertook the maintenance of the BALOR software in March of 2005. Since that time, various modifications have been made, primarily to improve processing efficiency. Recent efforts have focused on examining the propagation equations for consistency with the scientific literature, leading to a number of refinements. Furthermore, the capability to model a receiver at altitudes up to FL 400 has been added.

2 Groundwave Propagation Theory

2.1 Overview

BALOR calculates the complex attenuation W due to spherical, inhomogeneous, irregular terrain:

$$W = \frac{E_R}{E_0} \quad (1)$$

where E_0 is the primary field at the given observation position, assuming propagation through the atmosphere over a perfectly-conducting planar surface, and E_R is the actual received field. The phase of W represents the SF plus the ASF. By subtracting out the SF (the delay from propagation over a smooth, spherical, seawater path), BALOR then arrives at an estimate of the ASF.

Using the most general definition, ASFs include the effects of ground conductivity, changes in terrain elevation, receiver elevation, and temporal changes such as seasons, time-of-day, and local weather. BALOR models only the non-temporal factors.

For a comprehensive treatment of the subject of groundwave propagation, the reader is referred to [5]. In the sections that follow, we will present the key equations used in BALOR.

2.2 Propagation over a Smooth, Homogeneous, Spherical Surface

In order to model propagation over the surface of the earth, we start with the idealized case of a sphere having a smooth surface and uniform conductivity. The basic geometry is illustrated in Figure 1. Let the transmitter be a vertical current element at point A at height h_1 above point A', the projection of A onto the ground. Similarly, let the receiver be at point B at height h_2 above point B'. A' and B' are separated by an arc distance of d , subtending central angle θ . The radius of the earth is a .

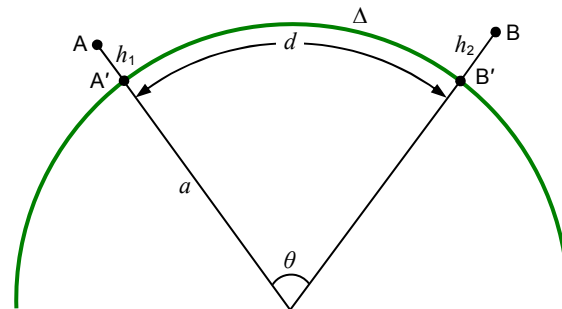


Figure 1. Geometry for propagation over a smooth, spherical earth. [Not to scale]

If the ground surface has conductivity σ_1 and permittivity ϵ_1 , then the *normalized surface impedance* Δ is defined as

$$\Delta = \left(\frac{k_0}{k_1} \right) \sqrt{1 - \left(\frac{k_0}{k_1} \right)^2} \quad (2)$$

where

$$k_0 = \omega\sqrt{\mu_0\epsilon_0} \quad \text{and} \quad k_1 = \sqrt{-j\omega\mu_0(\sigma_1 + j\omega\epsilon_1)} \quad (3)$$

Assuming for the moment that the transmitter and receiver are on the ground, the attenuation for this case may be specified by the “residue series”[6]:

$$W = \exp(-j\pi/4)\sqrt{\pi x} \sum_{s=1}^{\infty} \frac{\exp(-jxt_s)}{t_s - q^2} \quad (4)$$

where

$$x = A\theta, \quad q = -jA\Delta, \quad A = \left(\frac{k_0 a}{2}\right)^{1/3}, \quad \text{and} \quad \theta = \frac{d}{a} \quad (5)$$

The values t_s are complex roots to the differential equation

$$w_1'(t) - qw_1(t) = 0 \quad (6)$$

where $w_1(t)$ is in turn the solution to the second-order differential equation

$$\frac{\partial^2 w_1(t)}{\partial t^2} - tw_1(t) = 0 \quad (7)$$

The function $w_1(t)$ may be expressed using the Airy functions as

$$w_1(t) = \sqrt{\pi} [Bi(t) - jAi(t)] \quad (8)$$

or

$$w_1(t) = 2\sqrt{\pi} \exp(-j\pi/6) Ai[t \exp(-j2\pi/3)] \quad (9)$$

Although the summation in Eq. 4 has a limit of infinity, in practice the summation is evaluated until convergence is achieved; that is, until successive results are within a given tolerance. The series converges rapidly at longer distances, but poorly at shorter distances, requiring hundreds of iterations, and thus hundreds of roots t_s . See [5, Sec. 6.7] for an explanation of the process used to compute these roots. Note that it is very important for these values to be accurate.

Since the residue series converges poorly at shorter distances, a modified flat-earth solution [7] is used for ranges less than approximately 50 to 100 km:

$$W = \sum_{m=0}^{10} A_m [\exp(j\pi/4)qx^{1/2}]^m \quad (10)$$

where

$$\begin{aligned}
A_0 &= 1, & A_1 &= -j\sqrt{\pi}, & A_2 &= -2, & A_3 &= j\sqrt{\pi} \left(1 + \frac{1}{4q^3}\right), \\
A_4 &= \frac{4}{3} \left(1 + \frac{1}{2q^3}\right), & A_5 &= -\frac{j\sqrt{\pi}}{2} \left(1 + \frac{3}{4q^3}\right), & A_6 &= -\frac{8}{15} \left(1 + \frac{1}{q^3} + \frac{7}{32q^6}\right), \\
A_7 &= \frac{j\sqrt{\pi}}{6} \left(1 + \frac{5}{4q^3} + \frac{1}{2q^6}\right), & A_8 &= \frac{16}{105} \left(1 + \frac{3}{2q^3} + \frac{27}{32q^6}\right), \\
A_9 &= -\frac{j\sqrt{\pi}}{24} \left(1 + \frac{7}{4q^3} + \frac{5}{4q^6} + \frac{21}{64q^9}\right), & A_{10} &= -\left(\frac{32}{945} + \frac{64}{945q^3} + \frac{11}{189q^6} + \frac{7}{270q^9}\right)
\end{aligned} \tag{11}$$

In Loran terms, the phase of $W(\Delta, d)$ equals the total secondary phase delay, or SF + ASF. If Δ_0 is the normalized impedance for seawater, then the phase of $W(\Delta_0, d)$ is the delay over a seawater surface, or the SF. Now we can determine the ASF as the phase of $W(\Delta, d)$ minus the phase of $W(\Delta_0, d)$.

The phase delays obtained from Eq. 4 and Eq. 10 are plotted in Figure 2 versus distance for several values of ground conductivity. The plot on the left shows the total secondary phase delay, while that on the right shows the corresponding ASF values.

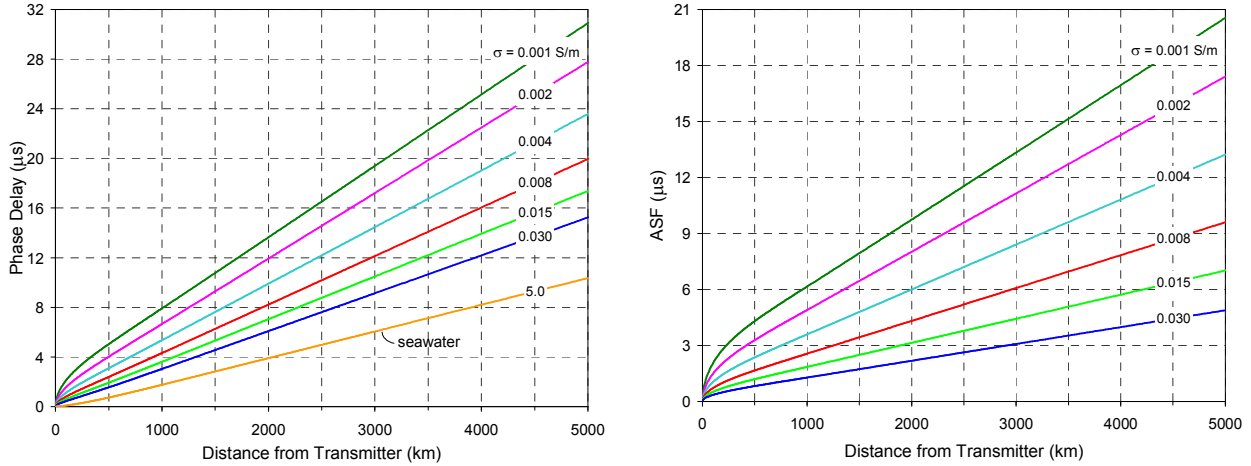


Figure 2. Phase of attenuation vs. distance for several values of ground conductivity: (left) absolute phase delay, and (right) additional secondary factor (ASF), which is phase delay relative to seawater.

2.3 Effective Earth Radius

In order to take into account the refractive properties of the atmosphere, a larger value, known as the *effective earth radius*, or a_e , is often used in place of the actual earth radius a . Thus the *effective earth radius factor*, or *eerf*, may be defined as

$$eerf = \frac{a_e}{a} \tag{12}$$

The inverse of this quantity is also commonly seen.

Traditionally, a value of 4/3 has been used for *eerf*. This quantity varies with frequency and ground conductivity, however, as shown on the left of Figure 3, taken from Rotheram [8]. Although *eerf* does

approach 4/3 at high frequencies, it also approaches 1 at low frequencies, and is somewhere in between at the Loran frequency of 100 kHz. BALOR provides a user option to use either 4/3 or 1.14 for $eerf$, the latter value being the approximate value of the seawater curve at 100 kHz. Johler and Berry [9] mention using a value of 0.9 for the inverse factor, which would result in a value of 1.11 for $eerf$ as defined above.

Phase delay curves for several combinations of $eerf$ and ground conductivity are shown in the plot on the right of Figure 3. Although the ground conductivity has a much larger effect on the phase delay than does the $eerf$ value, the effect of the latter is not insignificant, and becomes greater for longer distances and/or poorer conductivity.

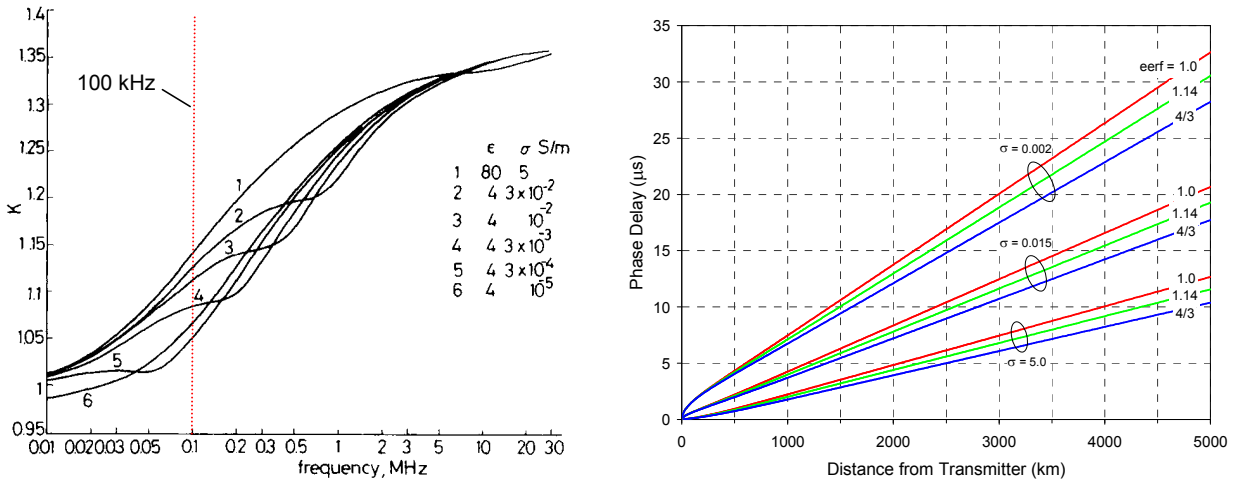


Figure 3. Effective earth radius factor: (left) $eerf$ as a function of frequency, and (right) the influence of $eerf$ on phase delay at several values of ground conductivity.

2.4 Induction Factor

Another quantity, commonly called the *induction factor* is often included as a factor in the attenuation equations to model near-field effects. This factor has the form:

$$induction\ factor = 1 + \frac{1}{jkd} + \frac{1}{(jkd)^2} = 1 - \frac{j}{kd} - \frac{1}{(kd)^2} \quad (13)$$

Figure 4 illustrates phase delay curves calculated using the residue series (Eq. 4) and the short distance formula (Eq. 10), with and without the induction factor. Seawater impedance was used; therefore these represent SF curves. Without the induction factor, the phase delay approaches zero as the distance from the transmitter approaches zero. On the other hand, with the induction factor, the phase delay approaches $5 \mu s$ as the distance gets small. The curve obtained from the polynomials given in the US Coast Guard's Loran Handbook [10] is also shown. It matches the classic curve with the induction factor quite well at most distances, but diverges rapidly at very short range.

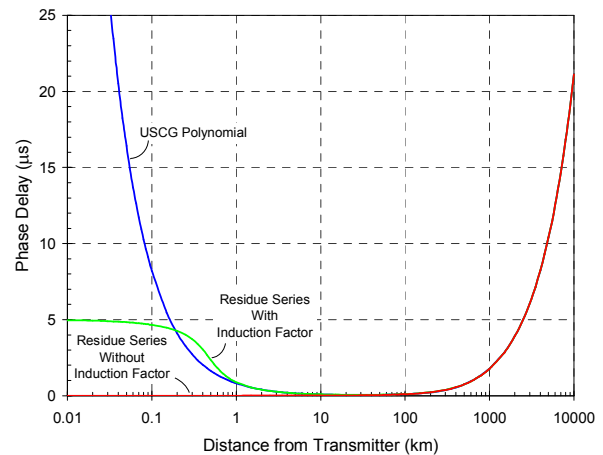


Figure 4. Phase delay curves for propagation over seawater with $eerf = 4/3$, showing the effect of the induction factor.

2.5 Propagation over a Smooth, Inhomogeneous, Spherical Surface

Now suppose that the surface impedance is not uniform, but varies as a function of position. This is known as an *inhomogeneous*, or *mixed-path*, case. The problem is initially represented in three-dimensional space, but can be reduced to a two-dimensional surface formulation through the use of boundary conditions. If we then make the simplifying assumption that any inhomogeneity occurs in the radial direction only, we arrive at the one-dimensional case illustrated in Figure 5. Here, the radial between the transmitter at A and the receiver at B may cross any number of regions, each having a discrete normalized surface impedance Δ_s .

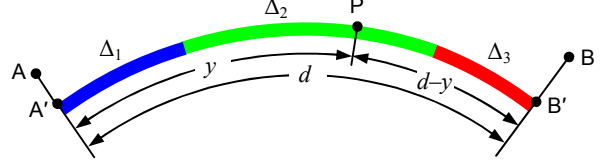


Figure 5. Geometry for propagation over inhomogeneous, spherical ground. [Not to scale]

Applying the compensation theorem [11], [12] produces the following expression for the attenuation factor over an inhomogeneous path:

$$W_P(d) = W_0(d) - \left(\frac{jd}{\lambda_0} \right)^{1/2} \int_0^d (\Delta_s - \Delta_0) W_P(y) W_0(d-y) \frac{dy}{[y(d-y)]^{1/2}} \quad (14)$$

where $W_0(d)$ is the attenuation for a homogeneous path of length d having reference normalized impedance Δ_0 , and $W_P(d)$ is the attenuation over the *perturbed* path; that is, the path with varying normalized impedance. $W_0(d)$ represents the attenuation over the forward path from the transmitter to the integration point P, whereas $W_0(d-y)$ represents the attenuation over the reverse path from the receiver to P. $W_0(d)$ and $W_0(d-y)$ may be calculated using Eq. 4 for long distances or Eq. 10 for short distances. The reference normalized impedance may be any constant value; but for our case, it is convenient to use seawater impedance.

In general, the above integral equation is still not directly solvable. If we assume that the integrand is smoothly varying, then numerical methods may be employed. We will use a method developed by Monteath [11].

Simplifying Eq. 14 somewhat by using the substitutions

$$b = \left(\frac{j}{\lambda_0} \right)^{1/2} \quad \text{and} \quad e_1(d, y) = (\Delta_s - \Delta_0) W_0(d-y) \quad (15)$$

gives

$$W_P(d) = W_0(d) - b \int_0^d e_1(d, y) W_P(y) \left[\frac{d}{y(d-y)} \right]^{1/2} dy \quad (16)$$

Now if the integration interval $[0, d]$ is divided into N intervals of equal length l , the integration can be approximated by a sum:

$$W_P(d_n) = W_0(d_n) - bl^{1/2} \sum_{i=0}^n C(n, i) e_1(d_n, d_i) W_P(d_i) \quad (17)$$

where $d_n = nl$, $d_i = il$, and n is an integer from 0 to N .

The coefficients $C(n, i)$ are given by

$$C(n, i) = \frac{J(i)J(n-i)}{J(n)} M(n, i) \quad (18)$$

where

$$J(k) = \begin{cases} 1 & \text{if } k = 0 \\ k^{-1/2} & \text{if } k > 0 \end{cases} \quad (19)$$

and $M(n, i)$ are weighting factors as provided in the following table:

n	$i = 0$	$i = 1$	$i = 2$	$i = 3$	$i = 4$	$i = 5$
1	1.14159	2.00000				
2	0.75605	2.07238	0.75605			
3	0.65170	2.73801	-0.40802	1.93606		
4	0.76430	2.13807	0.34003	1.26667	1.20000	
5	0.76430	2.22140	0.27860	0.89477	1.35000	1.20000

When n is greater than 5, $M(n, 0)$, $M(n, 1)$, and $M(n, 2)$ are the same as $M(5, 0)$, $M(5, 1)$ and $M(5, 2)$, respectively, while $M(n, n-2)$, $M(n, n-1)$, and $M(n, n)$ are the same as $M(5, 3)$, $M(5, 4)$, and $M(5, 5)$, respectively. For values of i greater than 2 and less than $n-2$, $M(n, i)$ is set to 1.

Bringing the last term outside the summation in Eq. 17, combining the terms in $W_P(d_n)$, and rearranging yields the following:

$$W_P(d_n) = \frac{W_0(d_n) - bl^{1/2} \sum_{i=0}^{n-1} C(n, i) e_1(d_n, d_i) W_P(d_i)}{1 + bl^{1/2} C(n, n) e_1(d_n, d_n)} \quad (20)$$

This is now a solvable, iterative equation. $W_P(d_0)$ is set to 1 to start, then the equation is evaluated in turn for $n = 1, 2, 3, \dots, N$. The solution for some $W_P(d_n)$ thus uses all of the previous $W_P(d_i)$, $i = 0, \dots, n-1$.

2.6 Propagation over an Irregular, Inhomogeneous, Spherical Surface

When the terrain elevations are varying over the radiation path, the ground is said to be *irregular*. This case may be solved in similar fashion to the smooth terrain case, with a few adjustments.

The reference normalized impedance Δ_0 is replaced by an *equivalent normalized surface impedance* Δ_e , defined by

$$\Delta_e = -\frac{E_{\theta 2}}{Z_0 H_{\phi 2}} \cos \alpha + \frac{E_{r 2}}{Z_0 H_{\phi 2}} \sin \alpha \quad (21)$$

where α is the slope angle of the terrain at a given point.

BALOR uses the far-field approximation:

$$\Delta_e \approx \Delta_0 \cos \alpha - \sin \alpha \quad (22)$$

Additionally, a factor of $\sec \alpha$ is introduced to account for the longer path over irregular terrain. With these changes, the compensation theorem equation may now be written as:

$$W_P(d) = W_0(d) - \left(\frac{jd}{\lambda_0} \right)^{1/2} \int_0^d (\Delta_s - \Delta_e) W_P(y) W_0(d-y) \sec \alpha \frac{dy}{[y(d-y)]^{1/2}} \quad (23)$$

where distances d and y are still arc distances measured along the smooth geoid as in Figure 5.

Equation 23 may be evaluated using the Monteath method as outlined in the previous section, substituting the following definition for $e_1(d, y)$:

$$e_1(d, y) = (\Delta_s - \Delta_e) \sec \alpha W_0(d-y) \quad (24)$$

2.7 Height Gain Factor

An expanded form of the residue series (Eq. 4) contains factors to model the effects of a raised transmitter and/or receiver. If the height of the transmitter is h_1 and the height of the receiver is h_2 , then the attenuation over a smooth, homogeneous, spherical surface may be calculated using:

$$W = \exp(-j\pi/4) \sqrt{\pi x} \sum_{s=1}^{\infty} \frac{\exp(-jxt_s)}{t_s - q^2} \frac{w_1(t_s - y_1)}{w_1(t_s)} \frac{w_1(t_s - y_2)}{w_1(t_s)} \quad (25)$$

where

$$y_1 = \frac{k_0 h_1}{A} \quad \text{and} \quad y_2 = \frac{k_0 h_2}{A} \quad (26)$$

and the remaining variables are as defined in Section 2.2. Note that if h_1 or h_2 is zero, the corresponding factor in Eq. 25 is reduced to one.

Since the gains from raising the transmitting antenna or the receiving antenna have the same form and (theoretically) are independent of one another, we may examine the generic height gain from raising one antenna while the other remains grounded. Let the height gain factor G_H be the ratio of the attenuation with a raised antenna to that with a grounded antenna, all other conditions being the same:

$$G_H(h, \Delta, d) = \frac{W(h, \Delta, d)}{W(0, \Delta, d)} \quad (27)$$

where h is the height of the antenna above the ground, d is the arc distance along the earth, and Δ is the normalized impedance of the surface.

The height gain turns out to be a complex function of height, conductivity, and distance. The magnitude of the height gain factor is shown for high and low ground conductivities in Figure 6. Each plot shows the function versus antenna height at various distances from the transmitter. Similarly, the phase of the height gain factor is shown in Figure 7.

An interesting observation is that the height “gain” may cause either an increase or a decrease in both magnitude and phase, depending on the conditions. Also, the function is essentially independent of

distance beyond 2000 km or so. The magnitude effects are more significant at longer distances, whereas the phase effects are more significant at shorter distances. The results may be somewhat questionable for the highest antenna heights and shortest distances, as the residue series was being pushed to its limits.

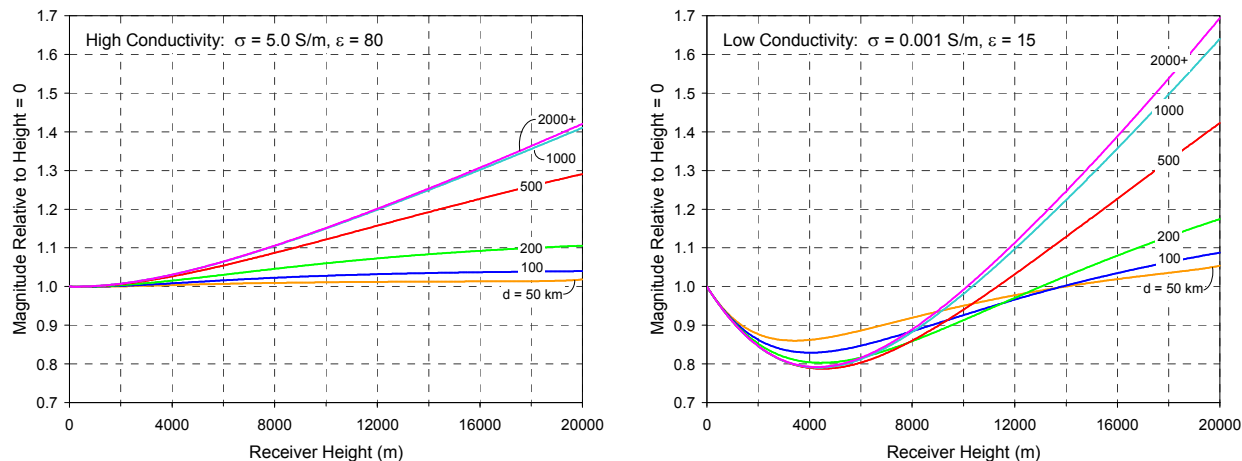


Figure 6. The effect of receiver height above ground on signal magnitude at various distances from the transmitter, shown for high ground conductivity (left) and low ground conductivity (right).

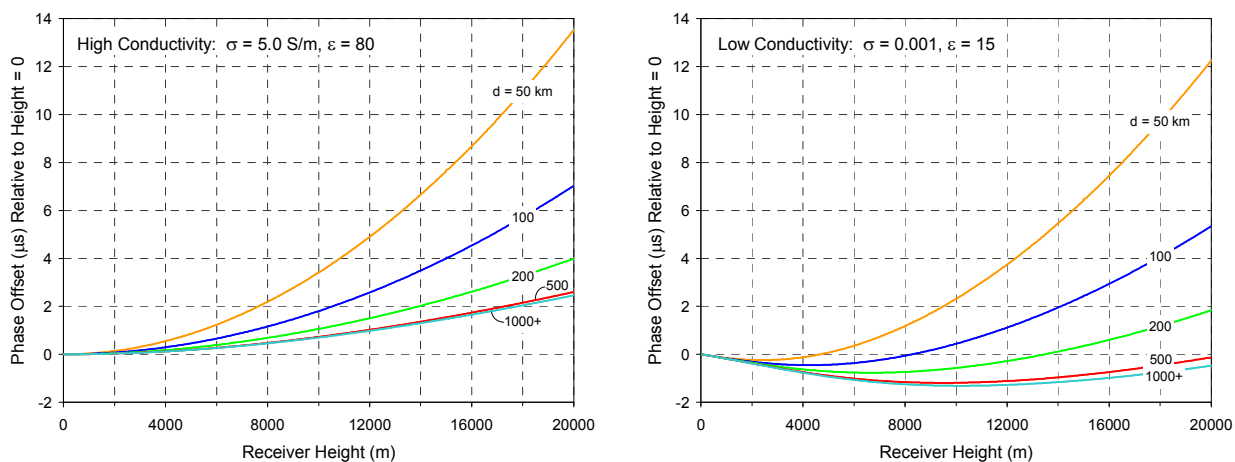


Figure 7. The effect of receiver height above ground on phase delay at various distances from the transmitter, shown for high ground conductivity (left) and low ground conductivity (right).

Now we wish to consider adding a raised receiver to the smooth inhomogeneous ground case. Recall that the solution involved the compensation theorem, as expressed in Eq. 14, and that this integral equation could be solved numerically using the Monteath method. So far, we have been assuming a grounded transmitter and receiver. Modeling a raised receiver is not as direct as simply plugging the receiver height into Eq. 25 when evaluating the function $W_0(d - y)$. Instead, the iterative Monteath method (Eq. 20) must first be carried out with the receiver on the ground at B', in order to determine all of the unknown values $W_P(d_n)$. Next one can iterate again, evaluating the attenuation for the raised receiver at B using the now known values of $W_P(d_n)$ in Eq. 17.

The situation becomes even more complicated for the irregular, inhomogeneous case (Eq. 23). A process similar to that described above is followed, but the receiver height must be adjusted for some sort of average terrain height.

3 Implementation Details

BALOR requires digital terrain elevation data (DTED) in order to model irregular terrain. See [13] for a description of the data format. Either Level 0 (900 m resolution) or Level 1 (90 m resolution) can be used. DTED Level 0 data may be downloaded from the National Geospatial-Intelligence Agency [14], whereas Level 1 data may be ordered on DVD from the USGS EROS Data Center [15].

Ground conductivity data was obtained from the Federal Communications Commission [16]. This data initially consisted of overlapping but incompatible files: M3.SEQ, which covered the continental US and some of the rest of North America, and R2.SEQ, which covered all of the Western Hemisphere. Both files were in vector format, designed to model the contour lines between conductivity zones, as illustrated in the map of the M3 region shown in Figure 8. A new ground conductivity file having a novel format was constructed from the merged data from both source files. Contour lines between conductivity zones are specified as chains of directed line segments having one conductivity value on the left and another on the right.

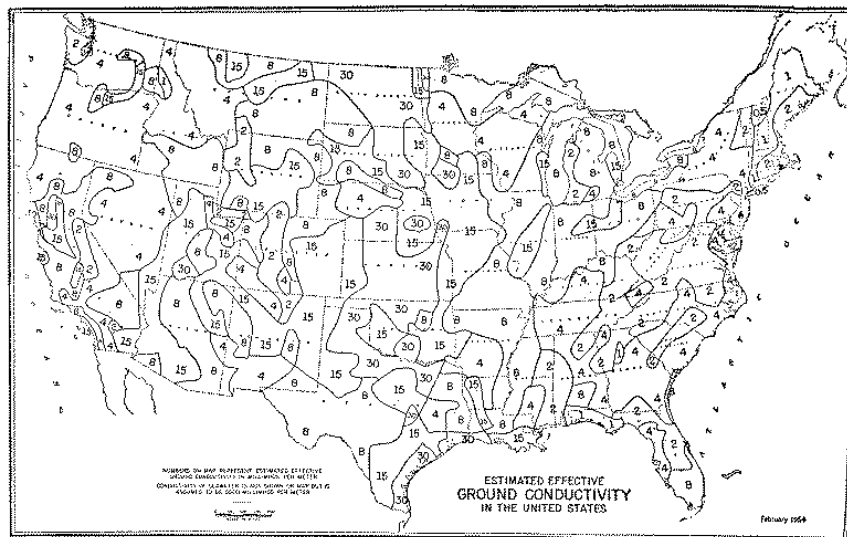


Figure 8. Map showing the ground conductivity zones for the continental US.

This vector-format ground conductivity database replaced the previous raster-format one. The conductivity profiles produced by BALOR now match the contours on the map much better, and any ambiguities caused by the use of a separate, non-directional coastline database have been eliminated. The fine level of detail provided by that coastline database has been lost, however; future plans therefore include merging more precise coastline data into the ground conductivity database, as well as adding data for the rest of the Loran world.

Forward and reverse distance and bearing calculations are carried out in BALOR using Vincenty's ellipsoidal methods [17]. Airy functions were implemented using algorithms developed by Amos [18].

A significant contributor to slow execution time was found to be the residue series (Eq. 4), which may need to iterate hundreds of times before converging, and which is itself placed inside a doubly-nested loop such that the inner loop may iterate on the order of a million times while processing a single radial.

In this application, the residue series, represented by W_0 in Eq. 14 or Eq. 23, always models propagation over smooth, homogeneous, seawater earth. Therefore, this function was simply digitized and replaced by an interpolated lookup table, resulting in a large performance gain with no loss of accuracy.

Similarly, the height-gain factor was not directly implemented in BALOR as in Eq. 25, since this form would have been prohibitively slow (the Airy function is also iterative). Instead, an approximate height-gain factor G_H was developed by empirical curve-fitting to Eq. 27, with the results described below.

First a preliminary gain factor that is independent of distance is calculated using

$$G_1(h, \Delta) = a_1 h k_0 \Delta + a_2 h^{5/2} k_0^2 \Delta + a_3 h^{5/2} k_0^2 \Delta^2 + a_4 h^2 k_0^{3/2} + a_5 h^{5/2} k_0^2 \quad (28)$$

where the complex coefficients a_n are given by

n	Real Part of a_n	Imaginary Part of a_n
1	-2.74333×10^{-2}	9.54401×10^{-1}
2	2.43025×10^{-4}	-1.78797×10^{-4}
3	1.26970×10^{-4}	1.28957×10^{-3}
4	7.20905×10^{-5}	-3.96662×10^{-5}
5	-1.46729×10^{-5}	-2.34672×10^{-6}

The final height gain is then obtained by applying a range factor:

$$G_H(h, \Delta, d) = \left[1 - \frac{h^{1/3}}{(1.2 \times 10^{-9}) d_C^2 + 24} \right] G_1(h, \Delta) + 1 \quad (29)$$

where d_C is the same as d , but constrained not to exceed 2500 km.

4 “Worst Case Path” Examples

Some real-world examples may help to illustrate the results of implementing the methods described above in the BALOR propagation model.

4.1 Path Description

Gambill and Schwartz described a propagation path dubbed the “Worst Case Path” [19], which makes a useful case study. This path extends 750 km along the radial from the Loran transmitter at Searchlight, NV, to Fort Cronkhite near San Francisco Bay, CA, traversing a variety of terrain, including the depths of Death Valley and the high peaks of the Sierra Nevada mountain range. Figure 9 shows a map of the Worst Case Path, together with a plot of the terrain elevation and ground conductivity profiles along this radial. It can be seen that the terrain is quite rugged, in addition to having an overall elevation change of 4300 m, and that the ground conductivity is quite varied as well.

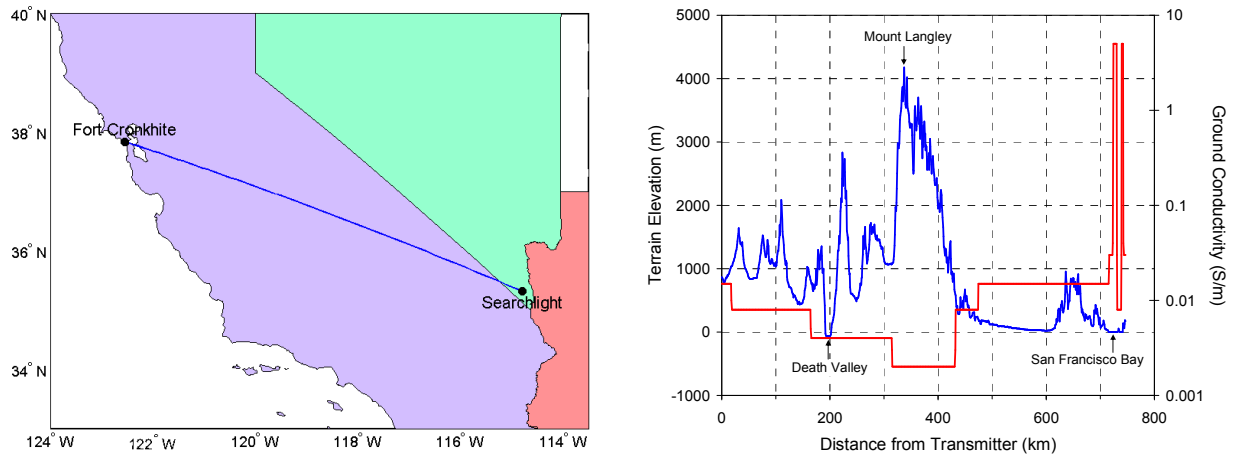


Figure 9. “Worst Case Path”: Map showing radial from transmitter at Searchlight, NV, to endpoint at Fort Cronkhite near the San Francisco Bay (left) and plot of terrain elevation and ground conductivity over this path (right).

4.2 Predicted ASF Values

Some predicted ASF values over this path, as calculated by BALOR, are presented in Figure 10. The upper trace shows the results obtained when all terrain elevations are set to zero, whereas the lower trace shows the results obtained when all conductivities are set to seawater values. The center trace shows the normal result; that is, both elevation and conductivity are considered.

ASF values tend to decrease on the side of a mountain facing the transmitter and to increase on the reverse side. The opposite effect is seen with a steep valley; for example, the ASF values increase and then decrease as the path crosses Death Valley at about 200 km from the transmitter. One can conclude, however, that despite the extreme terrain elevation changes over this path, the ground conductivity is a more significant factor in the final ASF values. Modeling the elevation changes contributes to the fine structure of the curve, and also causes a small overall decrease in the predicted ASF values.

4.3 Terrain Smoothing

When the terrain is especially rough, there may be excessive noise in the calculated results. Since the Loran wavelength is about 3 km, very small terrain features may safely be ignored. Figure 11 shows the effects of smoothing the elevation profile using a simple moving average calculation prior to modeling the ASFs. As well as reducing the noise, smoothing also increases the predicted ASF values somewhat. For the Worst Case Path example, Gambill and Schwartz used a smoothing interval of 6 km; Figure 10 was produced using an interval of 5 km.

It must be determined how much smoothing is acceptable; BALOR currently uses a default smoothing interval of 3 km, although this value may be modified by the user. When the terrain is gently rolling, the default level of smoothing has no discernible effect on the predicted ASF values.

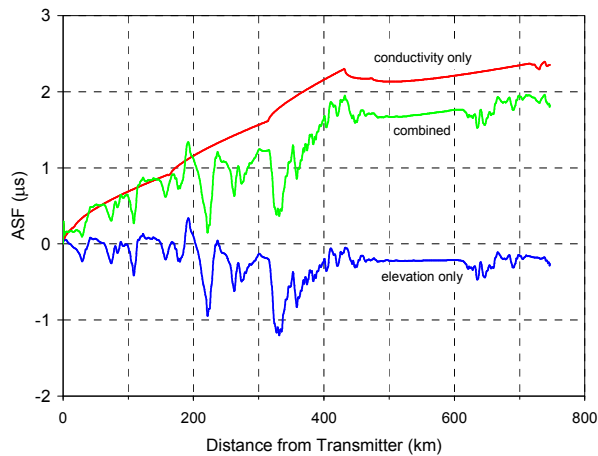


Figure 10. Contributions from ground conductivity and terrain elevation to predicted ASFs over the “Worst Case Path”.

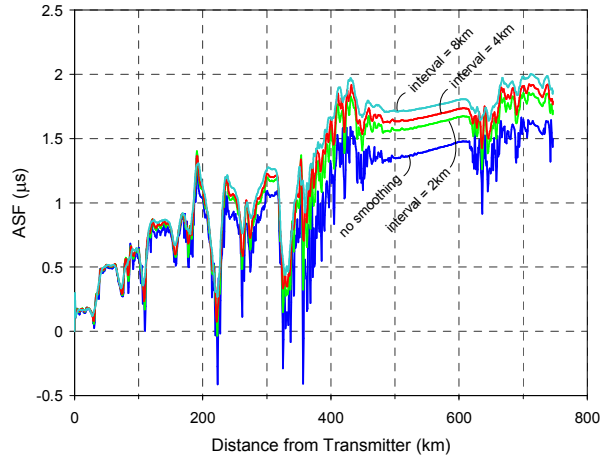


Figure 11. Effects of smoothing the terrain elevation profile on the predicted ASFs over the “Worst Case Path”.

4.4 Height Gain

The previous results apply to the case of a receiver at ground level. The effect of modeling an airborne receiver is illustrated in Figure 12. Due to the variations in ground conductivity, distance, and receiver height relative to the ground, the ASF offsets are not consistent. Raising the receiver may cause either an increase or a decrease in ASF values. This may be seen more clearly in the plot on the right in Figure 12, which shows, for receivers at various constant altitudes, the ASF offsets relative to the curve for a grounded receiver.

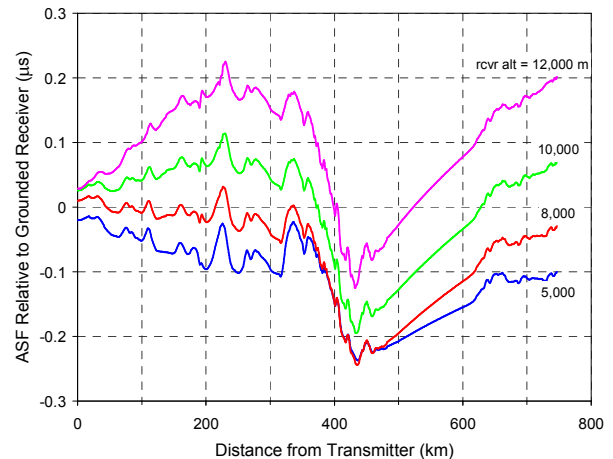
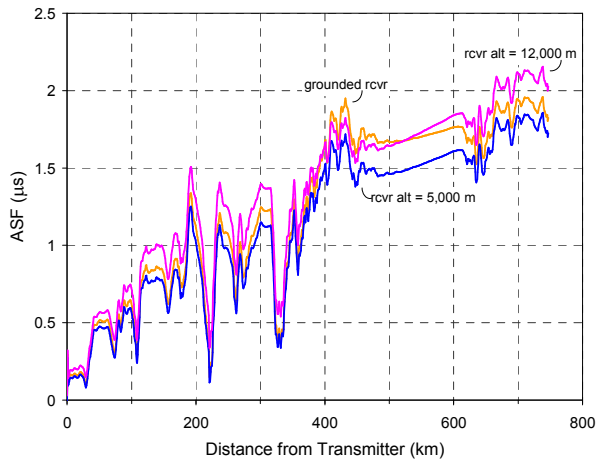


Figure 12. Effects of receiver altitude on predicted ASFs over the “Worst Case Path”: absolute ASFs are plotted on the left, while ASFs relative to a grounded receiver are shown on the right. Receiver altitude is with respect to mean sea level, while the height gain is calculated using the elevation above ground level.

5 Preliminary Validation Efforts

5.1 Comparison to Correction Table Values

The Loran Handbook [10] recommends the use of a set of tables called *Loran-C Correction Tables*, prepared and published by the Defense Mapping Agency [20]. These tables consist of ASF corrections to

measured time difference (TD) values for each master/secondary pair within each Loran chain. Values are given at intervals of five minutes of arc over the area that is both in range of the transmitters in question and within the US Coastal Confluence Zone. The accuracy of this data is not known.

The US West Coast chain (GRI 9940) with master station Fallon, NV, was selected as a test case, due to the rugged and varied regional terrain that has already been mentioned. Maps of ground conductivity and terrain elevation for the land area surrounding this chain are provided in Figure 13. These maps were produced by BALOR using its terrain databases. Note the low level of detail in the ground conductivity data relative to the elevation data. Close inspection also reveals that the conductivity values change at the US/Mexico border, illustrating the somewhat arbitrary nature of these values.

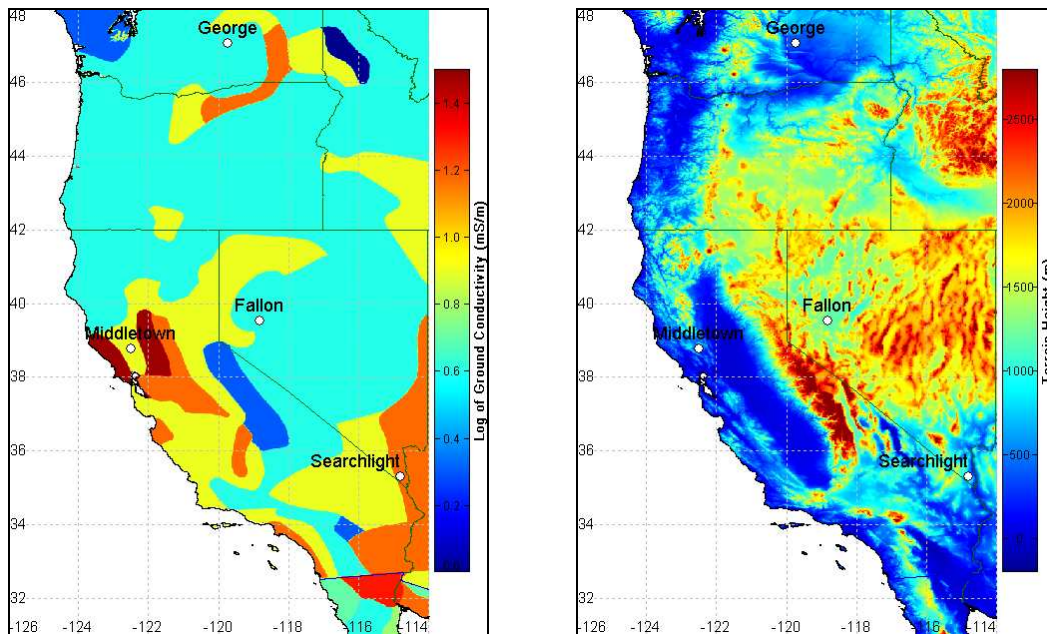


Figure 13. Ground conductivity (left) and terrain elevation (right) for the region of the US West Coast chain.

The ASF values calculated by BALOR are time-of-arrival (TOA) values. This basically means that they are *absolute* values for a single station. On the other hand, the ASF values provided by the tables are corrections to TD values; thus they are *relative* values for a master/secondary pair. It is a straightforward task to convert absolute ASF values to relative values comparable to the correction table values. The Fallon/Searchlight master/secondary pair was used as a test case.

First the absolute ASF values for each station were calculated separately, as illustrated in Figure 14. Next the ASF values for the secondary were subtracted from the corresponding values for the master. The resulting relative ASF values are plotted on the left in Figure 15, while the correction table values are plotted on the right. As far as can be determined by comparing the plots over the limited area covered by the correction table, the general trends match up well, with one important difference: the peak-to-peak spread of values is about one-third smaller for the BALOR-calculated results. (The scales have been adjusted in order to show the same color range in each plot; examining the range between minimum and maximum gives a quick estimate of amplitude differences between the cases.)

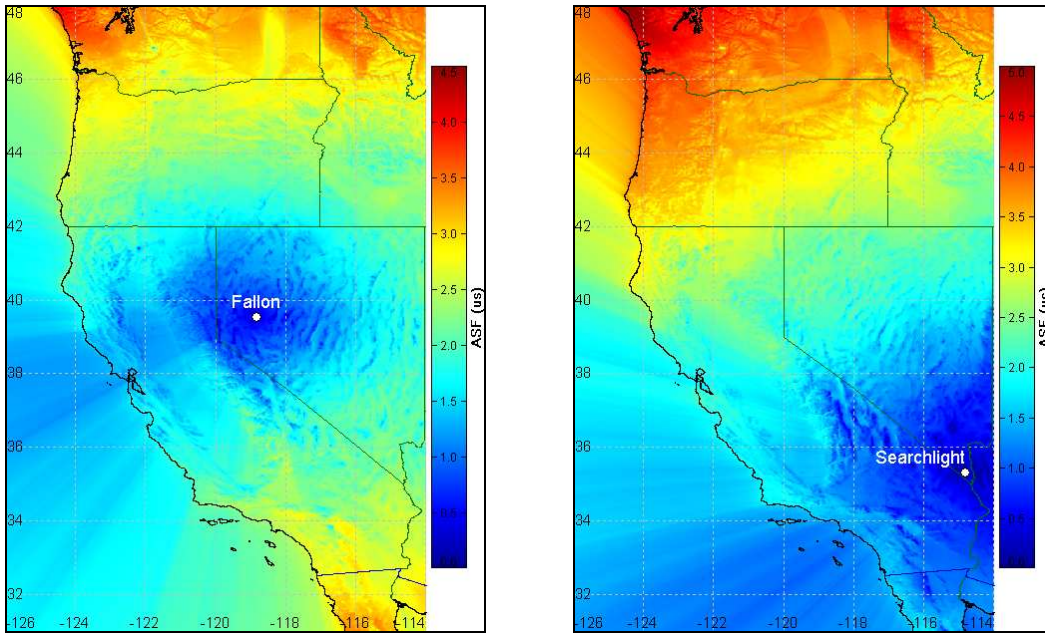


Figure 14. Predicted absolute ASFs over the US West Coast region for transmitters Fallon (left) and Searchlight (right).

The plot in the center of Figure 15 was obtained by repeating the BALOR calculations with all terrain elevations set to zero. Although the results in this case are smoother, the same overall trends are observed. The spread of values here is greater than with terrain elevations included, but it is still nearly one-fourth less than in the correction table case. As in the Worst Case Path example, it seems that including terrain elevation principally affects the fine structure of the results, while also causing a small overall decrease in predicted ASF magnitudes.

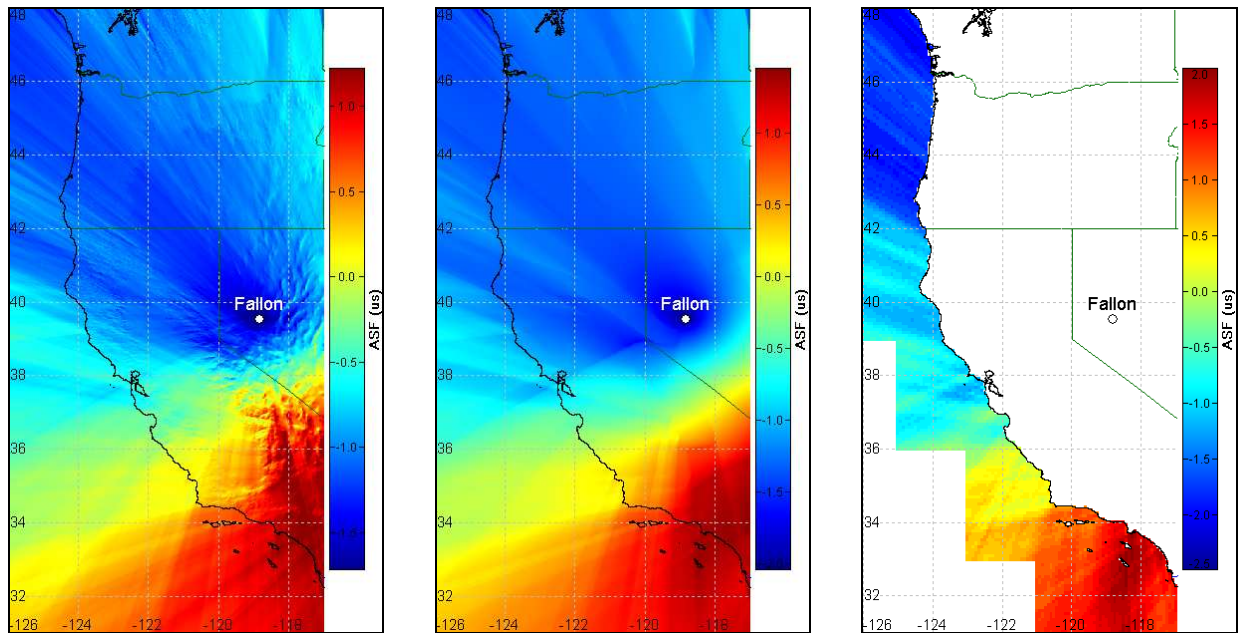


Figure 15. Relative ASFs for the Fallon-Searchlight pair: (left) predicted by BALOR using terrain elevation data; (center) predicted by BALOR using smooth earth; and (right) extracted from ASF Correction Tables. Note that Searchlight is beyond the eastern boundary of the maps.

5.2 Comparison to TOA Measurement System Flight Data

The TOA Measurement System (TMS), developed by Reelektronika, is designed to accurately measure the TOA of Loran signals with respect to UTC time derived from GPS. The system comprises Reelektronika's LORADD eLoran receiver, a NovAtel OEM-4 GPS receiver, a GPS-disciplined rubidium oscillator, an eLoran signal simulator, and other hardware, firmware, and software. See [21], [22], and [23] for details.

Use of the TMS enables the precise determination of the position of the Loran receiving antenna and the TOA of the Loran signals in terms of the same time standard. Since the precise time of transmission of the Loran signals is not known, however, the results are likely to show a small offset. The PF and SF are calculated from the known positions of the transmitter and receiver; then ASF values are calculated by subtracting PF and SF from the estimated propagation time.

The Avionics Engineering Center at Ohio University carried out flight campaigns over the eastern US in April and August of 2007 with TMS 2.0 installed in a King Air C90. As far as the TMS part of the mission was concerned, the main purpose was to test the operation of the system, rather than to validate BALOR. Nevertheless, two flight segments have been selected for preliminary validation checks.

The first flight segment is a radial flown from Ohio toward the transmitter at Carolina Beach, NC. This is plotted in Figure 16. The colors on the map represent predicted Carolina Beach ASF values for the entire region, as calculated by BALOR. Figure 17 shows the terrain elevation and ground conductivity profiles along this path. The first part of the path, in Ohio, is quite flat, while the middle part passes over the Appalachian Mountains, and the final part is sloping down toward sea level over rolling hills. The conductivity values do not vary widely, but are highest at the start and lowest over the mountainous terrain.

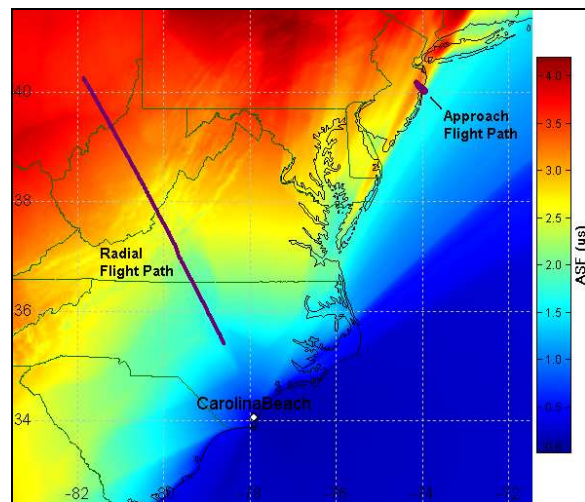


Figure 16. Map of the two flight segments discussed in the text, with the background showing the predicted ASFs from the Carolina Beach transmitter over the entire region.

The ASF values measured by the TMS over the radial path, together with the equivalent values predicted by BALOR, are plotted in Figure 18. It can be seen that although the general trend is the same, there are discrepancies between the two sets of results. The shape of the curves is different, and the highest ASF values differ by about 0.5 μs , or 12%. Some of the difference may be attributable to inaccuracies in the ground conductivity database or to seasonal variation.

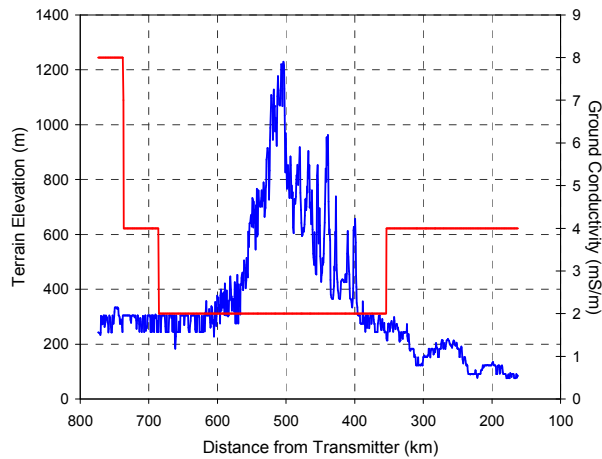


Figure 17. Terrain elevation and ground conductivity over the radial flight path.

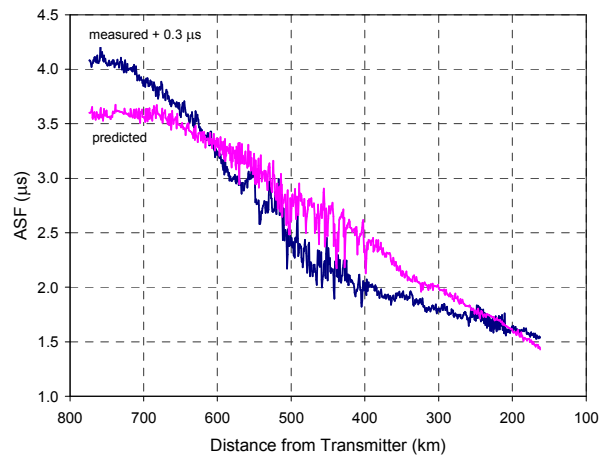


Figure 18. Measured and predicted ASF results for the radial flight path.

The second flight segment to be investigated is one of a series of approaches flown at Monmouth County Airport, Belmar/Farmingdale, NJ. This path is pointed out in Figure 16, and an enlarged view is shown in Figure 19. This particular segment is of interest because there is a large shift in ASF values over a relatively short distance. Examination of Figure 16 and Figure 19 reveals that a radial from Carolina Beach toward the eastern end of the path travels over considerably more ocean than a radial toward the western end. Since seawater is much more conductive than land, the ASF values are considerably lower for the part of the flight path that extends over the ocean.

The ASF values measured by the TMS over the approach path, together with the equivalent values predicted by BALOR, are plotted in Figure 20. Although the general shapes of the curves are similar, there are amplitude differences. The peak-to-peak change in ASF values is smaller for the BALOR results by about $0.4 \mu\text{s}$, or 25%. One possible factor is that the coastline data that BALOR is currently using is not very detailed. More precise coastline data is intended to be added in the near future.

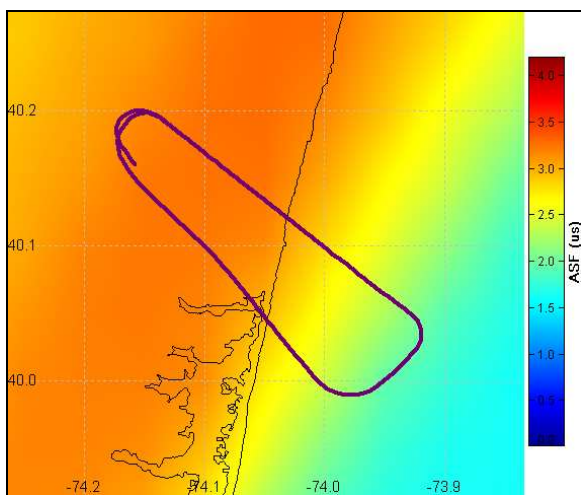


Figure 19. Enlarged view of the approach flight path over the New Jersey shore.

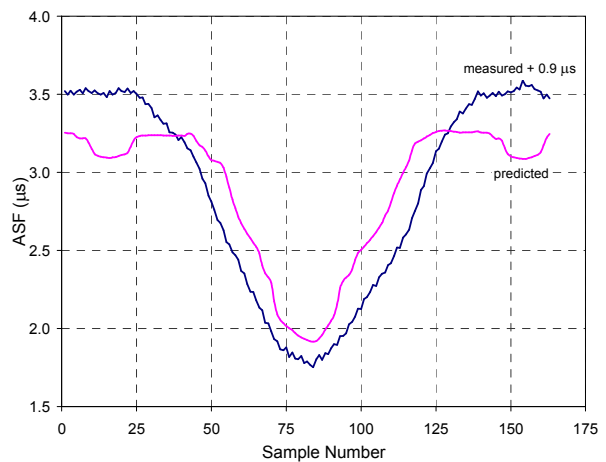


Figure 20. Measured and predicted ASF results for the approach flight path.

6 Conclusions

Accurate Loran navigation requires a good estimate of the pertinent additional secondary factors (ASFs). While these may be measured at select locations such as airports, it will be useful to have a model like BALOR that can predict ASFs over a large area. BALOR implements the classic methods for calculating propagation attenuation over an inhomogeneous, irregular, spherical earth, as described in this paper.

Recent modifications have improved BALOR's speed and reliability. Preliminary checks of predicted ASFs versus measured ASFs, however, seem to indicate that BALOR is underestimating the magnitude of the ASFs. Additional, methodical studies are needed to either validate the software or to determine what must be done to improve the predictions. Possible sources of error include: an inaccurate ground conductivity and coastline database; an incorrect value for effective earth radius factor (*eerf*); oversimplification in the development of the basic equations; errors in the implementation; and/or errors, offsets, or bias introduced by the measurement setup or data processing.

It should be noted that the current formulas used by Loran receivers in calculating the secondary factor (SF) are somewhat incorrect and inconsistent. First, an *eerf* of 4/3 seems to be universally used, but this value is almost certainly too high at Loran frequency. Second, various approximations to the seawater propagation curve are used, some of which are less accurate than others. And third, some of these curves incorporate the induction factor, while others do not. Any determination of ASF, whether by modeling or measurement, involves subtracting out the SF. Therefore, it is strongly recommended that a common method for calculating SF be adopted; otherwise, the usefulness of any predicted ASF values will be severely compromised.

7 Acknowledgments

The authors wish to thank Mitchell J. Narins of the Federal Aviation Administration, sponsor for this work; Dr. Paul Williams and Prof. David Last, creators of the BALOR computer program; and Reelektronika and Dr. Wouter Pelgrum, developers of the TOA Measurement System and related software.

References

- [1] D. Diggle, "Loran C accuracy considerations: terminal area and en route," Proceedings of the International Loran Association 35th Annual Convention and Technical Symposium (ILA-35), Groton, CT, Oct. 23-25, 2006.
- [2] R. Shalaev, G. Johnson, C. Oates, P. Swaszek, R. Hartnett, "The big picture on ASFs: The validity of predicted ASFs over long distances," Proceedings of the International Loran Association 35th Annual Convention and Technical Symposium (ILA-35), Groton, CT, Oct. 23-25, 2006.
- [3] D. Last, P. Williams, and K. Dykstra, "Propagation of Loran-C signals in irregular terrain – modelling and measurements: Part 1: Modelling," Proceedings of the International Loran Association 29th Annual Convention and Technical Symposium (ILA-29), Washington, DC, Nov. 13-15, 2000.
- [4] P. Williams and D. Last, "Extending the range of Loran-C ASF modelling," Proceedings of the International Loran Association 33rd Annual Convention and Technical Symposium (ILA-33), Tokyo, Japan, Oct. 25-27, 2004.
- [5] T. S. M. Maclean and Z. Wu, *Radiowave Propagation Over Ground*, Chapman & Hall, London, 1993.
- [6] J. R. Wait, "Recent analytical investigations of electromagnetic ground wave propagation over inhomogeneous earth models," *Proceedings of the IEEE*, vol. 62, Aug. 1974, pp. 1061-1072.
- [7] H. Bremmer, "Applications of operational calculus to ground-wave propagation, particularly for long waves," *IRE Transactions on Antennas and Propagation*, vol. AP-6, July 1958, pp. 267-272.

- [8] S. Rotheram, "Ground-wave propagation, Part 2: Theory for medium and long distances and reference propagation curves," *IEE Proceedings, Part F: Communications, Radar and Signal Processing*, vol. 128, Oct. 1981, pp. 285-295.
- [9] J. R. Johler and L. A. Berry, "Loran-D phase corrections over inhomogeneous, irregular terrain," Institute for Telecommunication Sciences and Aeronomy, Boulder, CO, IER 59-ITSA 56, Nov. 1967.
- [10] *LORAN-C User Handbook*, United States Coast Guard, Washington, DC, COMDTPUB P16562.6, 1992.
- [11] G. D. Monteath, "Computation of groundwave attenuation over irregular and inhomogeneous ground at low and medium frequencies," British Broadcasting Corporation, Kingswood, England, March 1978.
- [12] J. R. Wait, "The ancient and modern history of EM ground-wave propagation," *IEEE Antennas and Propagation Magazine*, vol. 40, Oct. 1998, pp. 7-24.
- [13] *Performance Specification Digital Terrain Elevation Data (DTED)*, National Imagery and Mapping Agency, Reston, VA, MIL-PRF-89020B, May 2000.
- [14] DTED Level 0 data are available for download at <http://geoengine.nga.mil/>.
- [15] DTED Level 1 data are available for download at <http://eros.usgs.gov/products/elevation.html>.
- [16] Ground conductivity data and maps are available for download at <http://www.fcc.gov/mb/audio/m3/>.
- [17] T. Vincenty, "Direct and inverse solutions of geodesics on the ellipsoid with application of nested equations," *Survey Review*, vol. 22, April 1975, pp 88-93.
- [18] D. E. Amos, "A portable package for Bessel functions of a complex argument and nonnegative order," *ACM Transactions on Mathematical Software*, vol. 12, Sept. 1986, pp.265-273. Paper and Fortran code are available for download at <http://doi.acm.org/10.1145/7921.214331>.
- [19] B. Gambill and K. Schwartz, "Loran-C signal analysis propagation model evaluation," General Electric (TEMPO), Santa Barbara, CA, GE78TMP-51, Contract DOT-CG-64810 A, Final Report, May 1978.
- [20] Loran-C correction table data and instructions are available for download at <http://nauticalcharts.noaa.gov/mcd/loranc.htm>.
- [21] *LORADD Series eLoran TOA Measurement System, LORADD-TMS, Installation and Operational Manual, v 1.0*, Reelektronika, The Netherlands, May 2007.
- [22] W. Pelgrum, A. Helwig, and D. Diggle, "Development, implementation, and verification of the TOA Measurement System," Proceedings of the International Loran Association 35th Annual Convention and Technical Symposium (ILA-35), Groton, CT, Oct. 23-25, 2006.
- [23] W. Pelgrum, "Loran TOA Measurement System 2.0: System enhancements, validation and shakedown," presented at the International Loran Association 36th Annual Convention and Technical Symposium (ILA-36), Orlando, FL, Oct. 14-17, 2007.

Biographies

Janet Blazyk is a Software Engineer with the Avionics Engineering Center at Ohio University, having joined the Center in 1990. Her work involves a variety of aviation-related computer applications, primarily in the areas of mathematical modeling and spectrum management. She holds an Sc.B. degree from Brown University and an M.S. degree in Mathematics/Computer Science from Ohio University.

Dave Diggle is the Associate Director of the Avionics Engineering Center at Ohio University in Athens, Ohio. In addition to his duties as Associate Director, he leads the LORAN Support Team at the Avionics Engineering Center. Dave is a member of the Institute of Navigation and the International Loran Association, and has received the RTCA's William E. Jackson Award for outstanding contributions in the field of avionics. He received his Ph.D. in Electrical Engineering from Ohio University and holds a private pilot certificate.